

A simple periodic peptide derived from *Pinctada fucata* Pif80 protein induces aragonite nucleation in magnesium absence

Bidisha Tah¹, Alexander Upcher² and Amir Berman^{1,2*}

1. Avram and Stella Goldstein-Goren, Department of Biotechnology Engineering, Ben-Gurion University of the Negev, Beer-Sheva, Israel
2. The Ilse Katz Center for Meso and Nanoscale Science and Technology, Ben-Gurion University of the Negev, Beer-Sheva, Israel

KEYWORDS . *Crystallization, template-directed, peptide, mollusk, Calcium Carbonate, Aragonite, Calcite*

ABSTRACT

Pif80 protein is associated with nacre formation in the Akoya pearl oyster. The influence of Pif2, a 32-mer peptide derived from Pif80, on calcium carbonate polymorphism, crystal orientation, morphology, and the induction of aragonite was investigated. X-ray diffraction (XRD) analyses reveal that Pif2, in the presence of a polydiacetylene (PDA) template, enhances calcite crystal nucleation on the (012) plane while suppressing the nucleation from the (104) face. Scanning electron microscopy (SEM) images illustrate the Pif2 concentration-dependent impact on calcite crystal morphology, with higher concentrations leading to deformed habits and distinct crystal faces. The peptide induces aragonite formation, even under conditions conducive to

calcite growth, as evidenced by SEM and transmission electron microscopy (TEM) studies, on the condition that an appropriate template is provided. Time-dependent SEM observations trace the transformation of amorphous calcium carbonate to calcite/aragonite, highlighting Pif2's role in this process. Experiments with geological aragonite templates affirm the preferential formation of aragonite in the presence of Pif2, as confirmed by TEM and focused ion beam scanning electron microscopy (FIBSEM) analyses. The results underscore Pif2's pivotal role in orchestrating the biological control of polymorphism in *Pinctada fucata*, providing valuable insights for biomineralization studies and biomimetic materials design.

INTRODUCTION:

Organisms from all five taxonomic kingdoms have the remarkable ability to form diverse and intricate inorganic mineral structures that serve various functions such as protection, support, grinding, and inorganic ion storage. Approximately 65 different biominerals have been identified, highlighting the wide range of mineralization processes in nature.^{1,2} Invertebrates, in particular mollusks, mineralize highly structured inorganic-organic composite materials, comprised mainly of calcium carbonate minerals, embedded in an organic matrix made of structural polysaccharides (chitin) and proteins.^{1, 3, 4} The manifestation of these properties is evident in the

precise selection of crystal phase, control of crystal orientation through directed nucleation, and the ordered assembly of organic-inorganic composite materials at multiple hierarchical levels.^{5,6} This is manifested in the precise selection of crystal phase, control of crystal orientation by directed nucleation, and ordered assembly of organic-inorganic composite materials in several hierarchical levels.^{1,7}

Biogenic calcium carbonate occurs mostly as the two stable anhydrous crystalline polymorphs: calcite (hexagonal) and aragonite (orthorhombic). A third polymorph, vaterite (hexagonal), is rarely found as a biomineral. There are some exceptions, such as in the carp inner-ear *Asteriscus otolith*,⁸ and freshwater mussel mixed aragonite-vaterite nacre-like lackluster pearls⁹. Additionally, the entire endoskeleton of the

tunicate *Herdmania momus* is composed of vaterite.^{10, 11}

Amorphous calcium carbonate, ACC, encompasses several hydrated, disordered phases that are widespread as transient phases, precursors to crystalline biominerals.¹² Stable ACC occurs in some crustacean exoskeletons and storage organs - gastroliths.^{13, 14, 15} Among the crystalline calcium carbonates, calcite is least soluble ($K_{sp}=10^{-8.48}$), aragonite solubility is comparable but somewhat more soluble ($K_{sp}=10^{-8.34}$), and vaterite is about tenfold more soluble ($K_{sp}=10^{-7.91}$).¹⁶ The less stable vaterite often transforms into calcite or aragonite in an aqueous solution in vitro.

Calcite is abundant among geological and biological minerals due to its stability with lower solubility product and Gibb's free energy than aragonite and vaterite.^{17, 18} Although pure aragonite is thermodynamically less stable than calcite, at normal pressures, about two-thirds of the CaCO_3 precipitated in modern oceans is aragonite; the rest is magnesian calcite, a solid solution of MgCO_3 and CaCO_3 .¹⁹ The $\text{Mg}^{2+}/\text{Ca}^{2+}$ ratio in the precipitation environment plays a pivotal role in determining the precipitated CaCO_3 phase. In modern oceans, the molar ratio of $\text{Mg}^{2+}/\text{Ca}^{2+}$ is 5:1, resulting in predominantly aragonite precipitation.¹⁹ Biomineral aragonite is found in all stony corals, in some marine turtle eggs²⁰ and Bivalve,²¹ Gastropod²² and Cephalopod (*Nautilus*)²³ mollusk shell nacre. In many cases, Bivalve mollusk shells are made of calcitic prismatic outer layer and aragonite nacreous inner layer^{24, 25} The prismatic layer prevents penetration due to its brittle and hard nature. In contrast, the nacreous layer shows high fracture toughness because of its hierarchical structure of organic lamina and inorganic aragonite.²⁶ Nacre crystal growth is guided by an array of macromolecules that are produced for specific purposes.

Soluble proteins extracted from mollusk shells have been demonstrated to influence the growth of CaCO_3 indicating their significant role in the shell formation process. These roles encompass directing crystal growth, selecting between calcite and aragonite phases^{27, 28} initiating crystal nucleation, and other functions, like attaching to the chitin framework, among others. They exert control over the formation of calcite and aragonite in mollusk shells and echinoderms.^{29, 30, 31, 32, 33, 34, 35}

It has been well established that acidic proteins play a major role in the organic matrix to regulate the stability, orientation, ACC transformation and polymorphism of CaCO_3 at the molecular level.³⁶ Approximately 72 different shell matrix proteins are secreted by *Pinctada fucata*.³⁷ Among them some are investigated, such as Aspein^{38, 39} AP7⁴⁰, AP24⁴¹, Pif97⁴², Pif80^{43, 44}, N16^{40, 45}, N25⁴⁶ etc. These proteins

predominantly regulate the lamellar sheets of the nacreous layer. Notably, Pif97 likely functions as a chitin-binding protein with the support of Pif80, along with N16, to induce the deposition of the aragonite chitin membrane in a specific c-axis orientation.⁴⁵

Suzuki et al. discovered an aragonite-specific binding protein in *Pinctada fucata*, Pif80, which is also bound to calcite crystals to some extent but more specifically to aragonite crystals.⁴⁴ However, only few studies of the effect of Pif80 have been reported to date.^{42, 43, 47, 44} Pif80 is likely an aragonite binding protein⁴⁸

In this work the effect a DDRK rich peptide, derived from Pif80 was studied and its effect on the aragonite formation was determined. Pif80 is at the C-terminal of Pif protein, consisting of Pif97 and Pif80 (AA 548-1007)⁴⁹. We have selected a 32-mer peptide from Pif80 with multiple DDRK consensus repeats, termed Pif2. The aim of this study is to determine whether Pif80, or this peptide can induce aragonite formation without Mg at room temperature on a suitable template.

MATERIALS AND METHODS:

10,12-Pentacosadiynoic-acid, $\text{CH}_3(\text{CH}_2)_{11}\text{C}\equiv\text{C}-\text{C}\equiv\text{C}(\text{CH}_2)_8\text{COOH}$; (PCDA) $\geq 97\%$ HPLC (Fluka), chloroform stabilized with Amylene (HPLC, Bio Lab Ltd. Israel). Ethanol, octadecyltrichlorosilane (OTS) 90+% (Aldrich), n-hexadecane oil ($\text{C}_{16}\text{H}_{34}$) 99% (Acros Organics), dichloromethane (CH_2Cl_2) $\geq 99\%$ (Sigma), Calcium Carbonate (CaCO_3) 99% (Sigma), CO_2 (Maxima), Calcium Chloride Dihydrate ($\text{CaCl}_2 \cdot 2\text{H}_2\text{O}$) extra pure (Merck), Sodium Carbonate (Na_2CO_3), and Sodium bicarbonate (NaHCO_3) 99.5% (Sigma). Distilled water (18.2 M Ω -cm) was obtained using a Millipore Reverse Osmosis filtration system. Peptide was derived from Pif80 (Pif2- DDRK DGR DDRK DRR DDRK DDRK G GK DDRK DDRK) by Novo Pep Limited. Geological aragonite Crystals (Morocco) from a gem shop.

2.1 Crystallization Procedure

Carbonate/bicarbonate buffer solution was prepared by mixing 25 mM Na_2CO_3 and NaHCO_3 at pH 10.2. Pif2 peptide solutions were added to 25 mM CaCl_2 solution to make final concentrations of 1, 2, and 5 mg/ml, with negligible change of CaCl_2 concentration. The $\text{Na}_2\text{CO}_3/\text{NaHCO}_3$ solution was combined with the CaCl_2 /peptide solutions in Eppendorf tubes with a pipette. 30 μl drops were promptly transferred to hydrophilic glass slides or to a PDA-coated glass slides for SEM observation. 2 μl drops were similarly employed to TEM grids. Reaction time ranged from 2 minutes to several hours. The glass slides or TEM grids were rinsed successively in DDW and ethanol to stop the reaction.

2.2 PDA Langmuir film preparation

PDA films were prepared using a Teflon Langmuir trough (Nima Technology Ltd., model 611), with dimensions of 7cm x 50cm, an area of 600cm², and a depth of 4mm, resulting in a volume of 240ml. The trough, equipped with movable barriers and a Wilhelmy plate surface pressure measuring system, was interfaced with a Nima 514 software. The trough was enclosed in a Perspex box to minimize dust and air movements. Ultra-pure water was used. 50 μ l of a 2mM PCDA (10, 12-Pentacosadiynoic acid (CH₃(CH₂)₁₁C \equiv C–C \equiv C(CH₂)₈COOH) solution in CHCl₃ was carefully, dropwise spread onto the water surface using a Hamilton 50 μ l syringe. The CHCl₃ solvent was left to evaporate for 15 minutes, leaving only the PCDA on the surface. PCDA was then surface compressed isothermally (at room temperature, 24 $^{\circ}$ C \pm 1 $^{\circ}$ C) by movable barriers at a constant rate of 20cm²/min. to form a 2D condensed phase. The target pressure was set to 20mN/m. Subsequently, UV irradiation of the compressed films was carried out using a hand-held UV lamp (λ =254nm) at 10cm above the film. This resulted in a polymerized "red phase" PDA layer, the color of which depended on the polymerization time. During UV irradiation, PDA polymerized into "blue" and "red" phases.^{50,51,52}

Following deposition and polymerization, the PDA Langmuir film in trilayer form was transferred to an octadecyltrichlorosilane (OTS) coated glass slide or TEM grid using the Langmuir-Schaefer technique.

2.3 Calcite morphology change

PDA was demonstrated to be an efficient template for calcite crystals on the (012) plane due to the close geometric match between the PDA tilted carboxylate and the carbonate orientation with respect to the nucleating plane. Also, there is close match between the periodic spacing of the polymer and calcite unit cell a direction, both nearly 5 \AA .^{53,54, 55} As a result the crystals are co-aligned with the single domain of the PDA film, where the crystals' \underline{a} axes are oriented parallel to the polymer backbone.⁵³

2.4 X-ray diffraction (XRD)

XRD was used as a tool to know the phase and orientation of the developed calcium carbonate crystals. Sample characterization was performed by X-Ray Powder Diffraction method. A Powder Diffractometer Empyrean (Panalytical B.V., Almelo, the Netherlands) equipped with a position-sensitive detector X'Celerator was used. Data were collected in $\theta/2\theta$ geometry using Cu-K α radiation (λ =1.542 \AA) at 40 kV and 30 mA. Scans were run for \sim 15 min in a 2θ range of 5-70 $^{\circ}$ with a step equal to \sim 0.033 $^{\circ}$.

2.5 Scanning Electron Microscope (SEM)

To know about the morphology of the sample HR SEM, JEOL JSM -7400F or XHR SEM, VERIOS 460L was used. The accelerating voltage for both instruments was

3.5kV with a working distance of 5 to 8 mm. For SEM, 30 μ l drops of growth solution were drop-casted on the piranha-cleaned or PDA-coated glass slide. The samples were coated with 4nm thick Pt or with carbon to reduce the electrical charging effect.

2.6 Transmission electron Microscope (TEM)

We have used TEM (JEM-2100F or JEOL JEM2011) as an essential tool to determine the crystal structure. Both microscopes were operated at an accelerating voltage of 200 kV. The JEM-2100F has a double-tilt sample holder with a Gatan Ultrascan 1000 2k x 2k camera. We used the Lacey 300 mesh Cu grid or Type-B continuous carbon grid for sample preparation. To see the cross-sectional view of the sample, TEM was followed by FIB.

2.7 Focused ion beam SEM (FIB-SEM)

The sample was treated in FIB (focused ion beam)/SEM (Helios G4 UC) to see the cross-sectional view of the geological crystal template with the overgrowth on it. 15 \times 2 μ m² area was covered by 0.5 μ m electron beam Platinum deposition to protect the film's surface from the Ga ions. Afterwards, the samples were milled around the protection layer, and then the region of interest was lifted out and attached to a TEM grid with a cross-sectional view parallel to the ion beam. Another protection layer was deposited on the surface of the lamella to protect and enable clean thinning of the sample. A probe of 39kV and then 5 kV were used for thinning samples from both sides and finally, the thickness was nearly 100nm, which is sufficient for TEM analysis.

RESULTS AND DISCUSSIONS

Calcite crystal orientation

Powder XRD was employed to examine calcite crystal orientation, as illustrated in Figure 1, nucleated on clean hydrophilic glass (trace A) and hydrophilic glass covered with a PDA monolayer (trace B). In the case of calcite nucleated on untreated glass, the crystals exhibited a random orientation, with diffraction peak intensities closely corresponding to the tabulated relative intensities.

Contrastingly, for calcite nucleated on PDA-covered glass, there was a noticeable increase in the intensity of the (012) peak, accompanied by a decrease in the intensity of the (104) peak. This intriguing observation implies a structural affinity between the surface structure and composition of the PDA film with the calcite (012) plane. This structural match indicates a lowered nucleation energy for the (012) plane, consequently enhancing calcite nucleation with a specific (012) orientation. This finding aligns with previous reports in the literature.⁵³

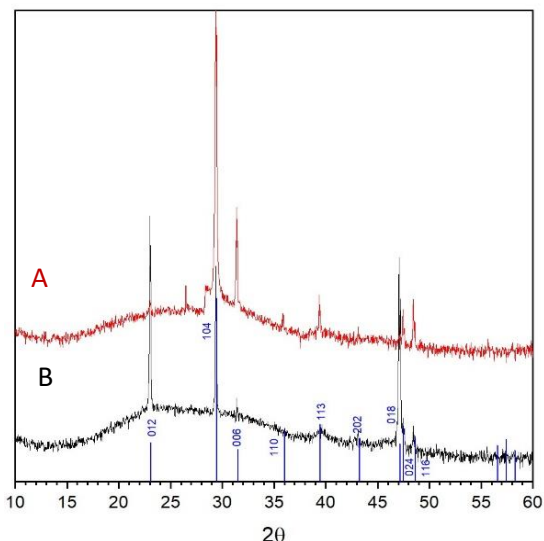


FIGURE 1: calcite XRD on Glass (A); The relative diffraction peak intensities closely correspond to the data file (bottom bars). Calcite nucleated on PDA (B) resulted in increased (012) and (018) and decreased (104) and other reflections relative intensities.

Calcite crystal morphology

Calcite crystals that nucleated on PDA in the absence of the Pif2 peptide displayed well-defined cleavage rhombohedron surfaces with smooth {104} faces, highlighting the evident (012) nucleating plane and the consistent alignment of crystals with the PDA template (see Figure 2A). As observed conventionally on PDA film, calcite crystals were uniformly aligned with the polymer's conjugated backbone.⁵³

In contrast, increasing concentrations of the Pif2 peptide during crystallization led to deformed calcite structures, as illustrated in SEM micrographs (see Figure 2B-G). New, coarse, and irregular faces emerged with approximate indices (011) ($0 < l < 2$). Notably, a distinct crystal face oriented upward, parallel to the nucleation plane, became prominent. With higher Pif2 concentrations and longer interaction times (Figure 2B, C – 1mg/ml, Figure 2D, E – 2mg/ml, Figure 2F, G – 5mg/ml), the crystals exhibited more significant deformation, and the newly formed faces were etched deeper into the crystal, leaving only residual unaffected {104} faces (Figure 2E, G - indicated by arrows). Figures B, D, and F depict crystals formed after 6 hours of reaction, while Figures C, E, and G represent crystals formed after 24 hours of reaction.

In the absence and presence of the Pif2 peptide, calcium carbonate precipitation on frosted glass resulted in non-oriented calcite. However, the presence of Pif2 induced the formation of increasingly deformed calcite crystals, exhibiting characteristic features reminiscent of those observed for PDA-templated calcite (see Scheme 1). Schematic diagram

1 provides a clear depiction of the impact of the Pif2 peptide on calcite crystals, leaving {104} faces unaffected.

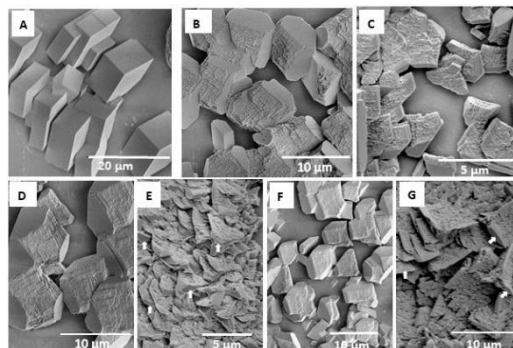
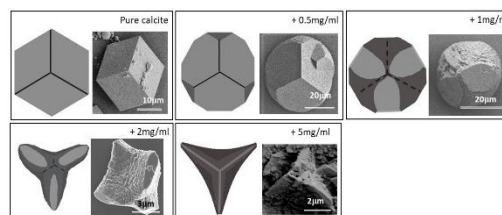


FIGURE 2: SEM images of calcite nucleated on PDA substrate, grown in 12mM CaCl₂ in the absence (Panel A) and presence of increasing Pif2 peptide concentrations and incubation times. Panel B&C, D&E, and F&G are calcite crystals grown in the presence of 1mg/ml, 2mg/ml, and 5mg/ml pif2., respectively. Panels A, B, D and F were incubated for 6 hrs. Panel C, E and G were incubated for 24 hrs. reaction time. Residual {104} facets are marked with white arrows in E and G.



SCHEME 1: Impact of Pif2 with varying concentrations on Calcite crystal formation

Induction of aragonite

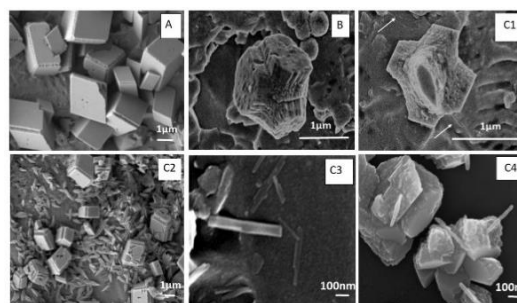


FIGURE 3: SEM images of calcium carbonate crystals grown on frosted microscope glass slide in peptide absence (A); in the presence of 2.0 mg/ml Pif2 (B) and 5.0 mg/ml Pif2 (C1); * mark the {104} faces. Images C2-C4 are from the same specimen at different locations and magnifications, depicting a mixture of calcite cleavage rhombohedra and aragonite needles (C1 arrows, C3, C4 arrows).

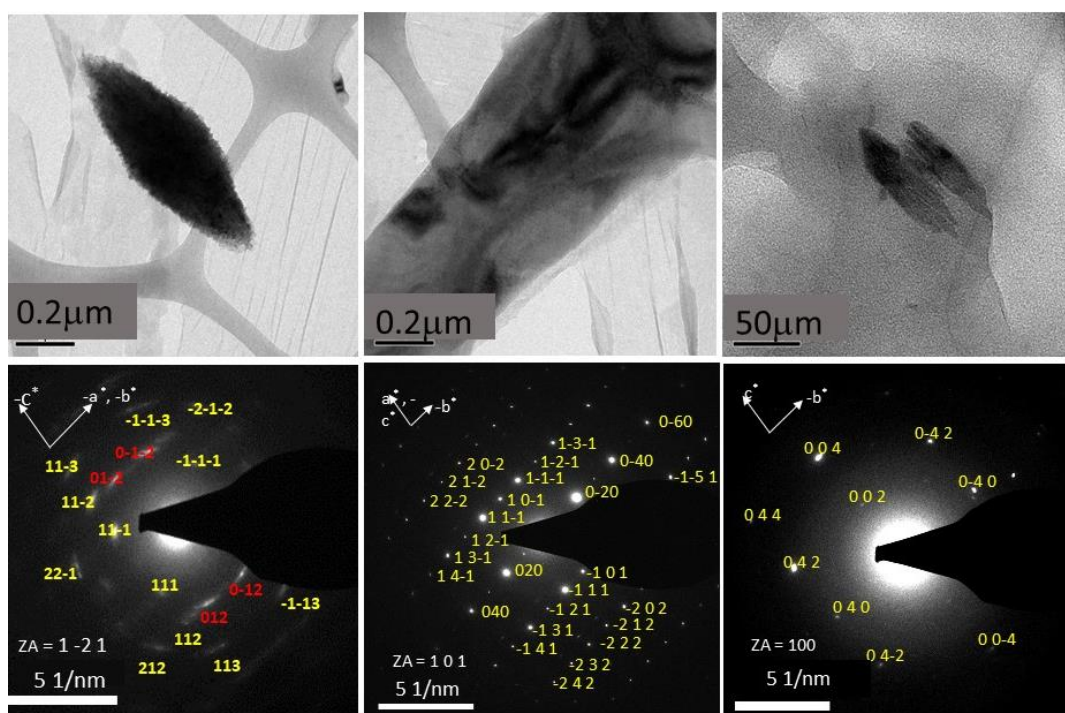


FIGURE 4 TEM micrographs (top) of oriented crystalline bundles (A), aragonite rod-like single crystals (B) and the initial stage of tiny aragonite bundles. The respective diffraction patterns are shown in the bottom Panels. All are at [Pif2]=5.0 mg/m

On the PDA substrate, deposited growth solution always nucleated calcite, whereas in PDA absence, aragonite was also observed. While the majority of the deposited CaCO_3 is calcite, at [Pif2]=2mg/ml - 5mg/ml, occasional aragonite needles and bundles are observed distributed unevenly on the sample, Figure 3.

Samples with crystalline needles, rods, and bundles, observed in SEM, Figure 3, were reproduced on TEM grids. Figure 4 depicts TEM micrographs and electron diffraction patterns of aragonite precipitation in the presence of 5.0 mg/ml Pif2, incubated for 60 min, then washed in DDW and ethanol. Figure 4A depict polycrystalline aragonite bundles oriented with zone axis $[\bar{1}\bar{2}1]$. Figure 4B (zone axis $[101]$) is a single crystalline rod-like structure of the type presented in Figure 3 C1-C4. Figure 4C depicts tiny polycrystalline bundles, showing the diffraction pattern of a single aragonite crystal with a zone axis $[100]$. These observations indicate that the presence of Pif2 peptide at sufficient concentration induces aragonite crystallization in the absence of Mg ions at room temperature.

To follow the crystallization pathway, we did a time-dependent study of the precipitates at short intervals, observed by SEM. The mixture of equimolar, 12.5 mM, $\text{Na}_2\text{CO}_3/\text{NaHCO}_3$ (2:1) and CaCl_2 (pH=10.2) was prepared and drop-casted on glass slide. The reactions were stopped after 2 minutes, 5 minutes, 10 minutes, 20 minutes, and 30 minutes, rinsed in water and ethanol, and imaged in SEM (Figure 5). Figure 5A (2 min) shows only a few scattered precipitates at the onset of precipitation. At 5 min (Figure 5B), hundreds of uniform spherical objects, ca. 100-200 nm radius, are clustered. Similar clusters analyzed in ED indicate its amorphous structure. An EDS was performed to confirm the chemical composition of these particles. From the spectrum of EDS (Inset image), we confirmed that those particles are calcium carbonate. There, the platinum peaks come from the platinum coating made on the glass slide. From literature⁵⁶ it is well known that amorphous calcium carbonate (ACC) structures are spherical particle having size less than 1 mm reveal that those spherical particles formed after 5min of reaction are ACC. Interestingly, the SEM images show that those ACC particles accumulated and crystallized

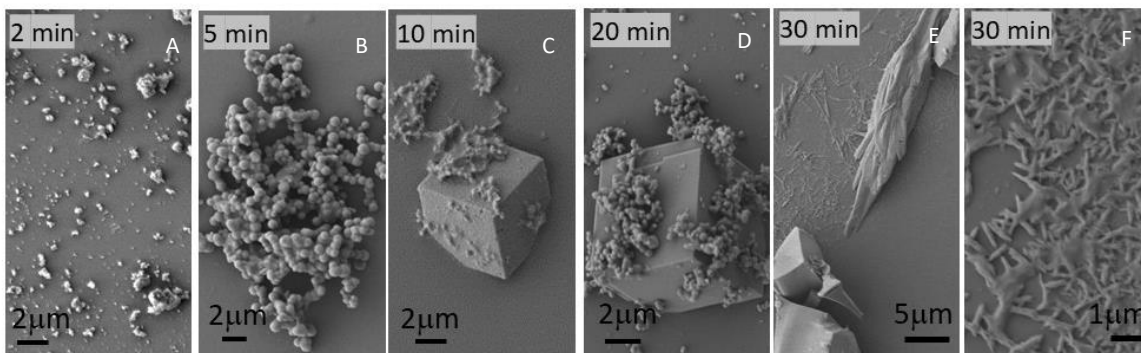


FIGURE 5: SEM images of calcium carbonate growth kinetics on glass in the presence of 2 mg/ml pif2, at (C), 20 min. (D), and 30 min. (E and F).

into calcite during the reaction time of 10 to 20 minutes. SEM images show that after 30 minutes of reaction, there is a mixture of calcite and bundles of aragonite. Due to the effect of peptide, those calcites are defective, and aragonite is formed. The defect on the calcite made by the peptide is also very prominent. The initial stage of Aragonite bundles are hard to find in these SEM images because of their tiny size (Figure 3, Panel C1, indicated by arrow). This kinetic study

reveals that the ACC is transforming into calcite/aragonite and peptide plays the role for the defected calcite and aragonite bundles.

Still, now, we observe that a higher amount of peptide produces bundles or rod-like aragonite along with the defective calcite on the glass substrate as well as Cu grid. Considering the critical effect of templates on

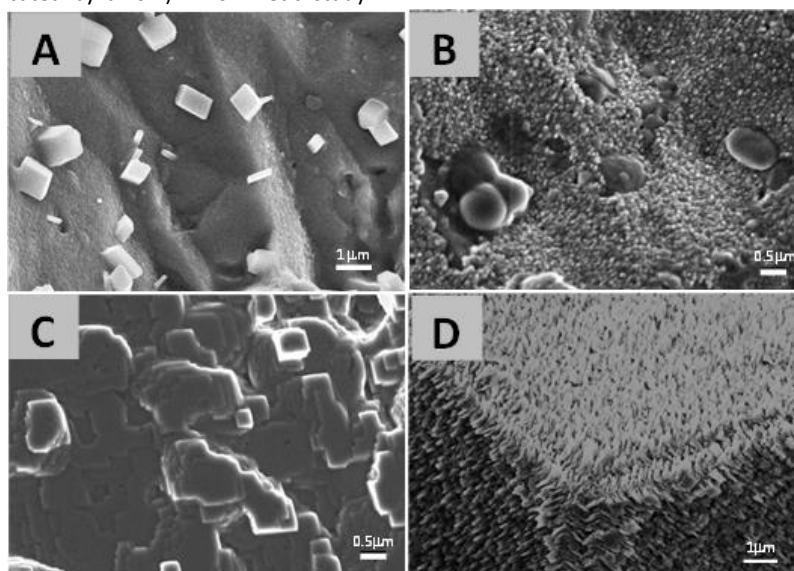


FIGURE 6: SEM images of calcium carbonate overgrowth (A) on geological (001) aragonite surface in Pif2 absence, resulting in randomly oriented calcite (B). CaCO_3 on aragonite (001) face with 5mg/ml Pif2 results in epitaxial overgrowth of oriented aragonite (B). In contrast, CaCO_3 overgrowth on geological (104) calcite surface in Pif2 absence resulted in oriented rhombohedral morphology (C). Overgrowth on (104) calcite faces (viewed along the c axis) in the presence of 5mg/ml Pif2 resulted in epitaxial calcite sub-micron protrusions (-D).

crystallization, orientation and specially the phase of the crystals depend on the type of template,^{57,24} we have performed in parallel the same crystallization experiments on the of the geological aragonite plane (001) and calcite plane (104) templates. Figure 6A (without Pif2) and 6B (Pif2 5 mg/ml) depict SEM images of calcium carbonate crystals nucleated on geological

aragonite. In contrast, figure 6C and D depict the calcium carbonate crystallized on geological calcite crystal. In the absence of peptides, a few calcite crystals are randomly oriented on the geological aragonite surface. Whereas, in the presence of peptide (Pif2 5mg/ml) SEM Figure-6 (Panel-B) shows the overgrowth on the surface of geological aragonite and

very few deformed calcite crystals. Very interestingly, these overgrowths are mostly all over the surface. However, we need to confirm the phase of these overgrowths. On the other hand, as usual, the calcite crystals are formed without peptides (Panel C) on the

geological calcite surface. However, in the presence of peptide (5mg/ml), the surface becomes affected mostly along the C axis of the geological calcite crystal

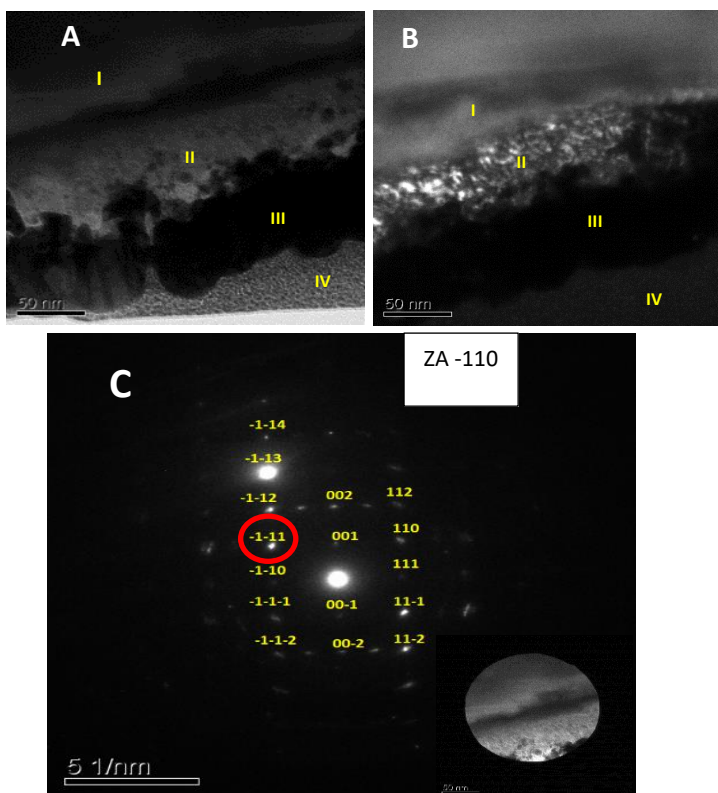


FIGURE-7: TEM imaging followed by FIBSEM (Focused Ion Beam Scanning Electron Microscope). Panel A and B are the TEM images of bright and dark fields, respectively, where the four different regions are clearly identified. Region I is the substrate of geological aragonite. Region II is the overgrowth on the surface of the geological aragonite. Region III and IV are the Ag and Pt layers deposited to make the sample conductive during SEM. Panel C (Image 7) shows the SAED pattern of regions I and II (the Inset Image shows the aperture for the diffraction)

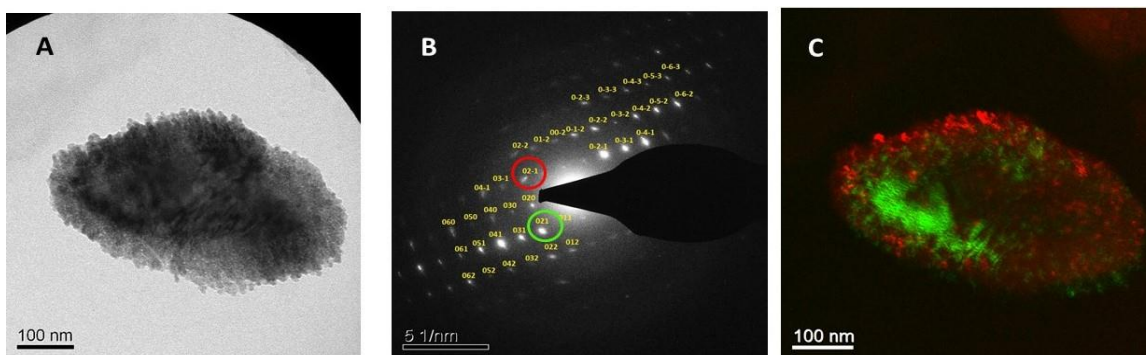


FIGURE 8: TEM Bright Field Imaging (A) of Crushed Geological Aragonite with Overgrowth, SAED Pattern (B), and Dark Field Images from (021) and (02 $\bar{1}$) Reflections (C). The green and red color areas originate from the red and green circled circles (B), respectively.

To confirm the phase of the precipitation on the surface of geological aragonite (Figure 6B), we did TEM imaging (Figure 7) followed by FIBSEM (Focused Ion

Beam Scanning Electron Microscope). Figure 7A is a bright-field TEM image, where the four different regions are very clearly identified. Region I is the

substrate of geological aragonite, Region II is the overgrowth on the surface of the geological aragonite, Region III and IV are the Ag and Pt layers deposited for making the sample conductive during SEM. Panel C (Image 6) shows the SEAD pattern of the region I and II (Inset Image shows the aperture for the diffraction).

The SEAD pattern obtained through TEM (Figure 7C) confirmed the observed overgrowth on geological aragonite crystals is also aragonite. The single crystal diffraction pattern examination revealed that the This finding emphasizes the role of Pif2 in promoting aragonite formation over calcite. Even under conditions favorable for calcite growth (i.e., without Mg and at room temperature), the aragonite template reduces the barrier energy for crystal nucleation, underscoring Pif2's influence on the preferential formation of aragonite.

Geological aragonite crystals were finely crushed and used as a template to validate this further. Ground aragonite particles were placed on a TEM-Cu grid, and a growth solution mixture with 5mg/ml Pif2 was drop-casted on the crushed aragonite crystals, allowing the reaction to proceed for 12 hours.

In Figure 8A, the TEM image illustrates that the geological aragonite crystals are covered with overgrowth aragonite crystals. The SEAD pattern in Figure 8B matches well with the aragonite diffraction spot with the zone axis (100), indicating that the overgrowth is well-aligned with the core geological aragonite crystal. The single crystal-like diffraction pattern reveals that the bright and broad spots signify the thicker region, representing the core geological aragonite crystal. In contrast, the sharp and lighter spots correspond to the thinner and smaller crystalline area, representing the overgrowth.

This observation is further confirmed through dark-field superimposed TEM imaging (see Figure-8C), where the illumination of the (0 2 1) reflection (encircled in green in Figure 8B) confirms diffraction from the core geological crystal, whereas the illumination of (0 2 -1) reflection (encircled in red in Figure 8B) confirms diffraction from the overgrowth aragonite crystals, demonstrating their alignment with the core aragonite crystal.

This observation reiterates that Pif2 nucleates aragonite crystals when the template favors aragonite formation under calcite-favorable growth conditions.

Calcite can be easily synthesized due to its thermodynamic stability under atmospheric temperature and pressure conditions. In contrast, aragonite represents a metastable phase. The energy barrier to aragonite nucleation is greater than to calcite in the absence of additives. Aragonite therefore only forms under reaction conditions that either actively promote its nucleation or inhibit calcite

nucleated aragonite on the geological aragonite crystals is well-aligned with the zone axis [-1 1 0].

This confirmation was further substantiated through dark-field TEM imaging (Figure-7B), where the illumination of the (-1 -1 1) reflection (encircled in Figure 7C) confirmed that this spot originated from the overgrowth. Those comprise well-aligned aragonite crystals nucleated on the geological aragonite core crystal.

formation (as occurs with magnesium ions).⁵⁷ It is challenging to generate aragonite without Mg in an aqueous medium at room temperature. Research by Wray and Daniels⁵⁸ indicates that the temperature promotes the formation of aragonite and vaterite. Investigations by Lippman¹⁸, {Kojima, 1994 #5042} explore the impact of temperature on aragonite formation, comparing nucleation and crystal growth rates of calcite and aragonite from supersaturated solutions. However, the Mg²⁺ ion is known to favor the synthesis of aragonite at high concentrations.¹⁸ Ostwald's rule indicates that numerous polymorphic compounds undergo crystallization through progressively more stable phases. This phenomenon is believed to occur when the energy barriers associated with the formation of each metastable phase are lower than the barrier leading directly to the most stable phase.⁵⁹ In the context of calcium carbonate, however, Ostwald's rule is not consistently followed. Specifically, aragonite does not serve as a precursor to calcite under ambient conditions. This deviation highlights that, despite their close thermodynamic stability, the energy barrier for aragonite nucleation surpasses that for calcite in the absence of additives. As a result, aragonite only emerges under reaction conditions that actively foster its nucleation or impede calcite formation, as observed with magnesium ions.

Our findings reveal that an increased concentration of the peptide Pif2 (5 mg/ml) promotes the development of aragonite while simultaneously suppressing calcite nucleation. Conversely, a lower concentration of Pif impacts calcite crystals, with a noticeable emphasis on a distinct crystal face oriented upwards, parallel to the nucleation plane. In the presence of an appropriate template, specifically the geological aragonite crystal surface, under room temperature conditions, in the absence of Mg, and a concentration of 5 mg/ml Pif2, all nucleated crystals exhibit the aragonite phase and are perfectly aligned with the template. In this scenario, a similar kind of template and Pif2 as an additive reduce the barrier energy for aragonite nucleation, facilitating the production of aragonite. The Pif2 peptide's origin from the aragonite binding protein Pif80 in *Pinctada fucata*,⁴⁴ characterized by a sequence of neutrally charged repeating amino acids ('DDRK'), underscores its pivotal role. Our results affirm and underscore the significance of the Pif2

segment within the Pif80 protein in governing the biological control of polymorphism in *Pinctada fucata*.

CONCLUSIONS

In conclusion, the study elucidates the intricate role of the Pif2 peptide in controlling calcium carbonate polymorphism. The findings demonstrate that Pif2 promotes aragonite development and alters calcite crystal morphology. The peptide's influence is evident even under conditions favoring calcite growth, showcasing its ability to override thermodynamic stability.

The research underscores the significance of Pif2 as a key player in the biological control of polymorphism in *Pinctada fucata*. The peptide's impact on crystal orientation, morphology, and the induction of aragonite provides valuable insights into the complex interplay between biomolecules and mineralization processes.

REFERENCES:

1. Lowenstam, H. A.; Weiner, S., *On Biomineralization*. Oxford University Press: Oxford New York, 1989.
2. Mann, S., Oxford University Press: New York, 2002.
3. Weiner, S.; Dove, P. M., An overview of biomineralization processes and the problem of the vital effect. *Rev. Mineral. Geochem.* **2003**, 54 (1), 1-29.
4. Weiner, S.; Addadi, L., Design strategies in mineralized biological materials. *J. Mater. Chem.* **1997**, 7 (5), 689-702.
5. Meyers, M. A.; McKittrick, J.; Chen, P.-Y., Structural Biological Materials: Critical Mechanics-Materials Connections. *Science* **2013**, 339 (6121), 773-779.
6. Weiner, S.; Addadi, L.; Wagner, H. D., Materials design in biology. *Materials Science & Engineering C-Biomimetic and Supramolecular Systems* **2000**, 11 (1), 1-8.
7. Mann, S., *Biomineralization: Principles and Concepts in Bioinorganic Materials Chemistry*. Oxford University Press: 2001.
8. Li, Z.; Gao, Y.; Feng, Q., Hierarchical structure of the otolith of adult wild carp. *Materials Science and Engineering: C* **2009**, 29 (3), 919-924.
9. Qiao, L.; Feng, Q.-L.; Li, Z., Special Vaterite Found in Freshwater Lackluster Pearls. *Crystal Growth & Design* **2007**, 7 (2), 275-279.
10. Kabalah-Amitai, L.; Mayzel, B.; Zaslansky, P.; Kauffmann, Y.; Clotens, P.; Pokroy, B., Unique crystallographic pattern in the macro to atomic structure of *Herdmania momus* vateritic spicules. *Journal of Structural Biology* **2013**, 183 (2), 191-198.

Overall, the study contributes to our understanding of how specific peptides, derived from aragonite binding proteins, can regulate the crystallization of calcium carbonate polymorphs. These findings have implications not only in the field of biomineralization but also in materials science and the design of novel biomimetic materials with controlled crystal structures.

ACKNOWLEDGEMENTS

We want to thank to Kreitman School of Advanced Graduate Studies for funding and Ilse Katz Institute for Nanoscale Science & Technology department for the technical facilities. Thanks to Nili Ben-shushan for insightful discussions.

11. Kabalah-Amitai, L.; Mayzel, B.; Kauffmann, Y.; Fitch, A. N.; Bloch, L.; Gilbert, P. U. P. A.; Pokroy, B., Vaterite Crystals Contain Two Interspersed Crystal Structures. *Science* **2013**, 340 (6131), 454-457.
12. Addadi, L.; Raz, S.; Weiner, S., Taking advantage of disorder: Amorphous calcium carbonate and its roles in biomineralization. *Advanced Materials* **2003**, 15 (12), 959-970.
13. Al-Sawalmih, A.; Li, C.; Siegel, S.; Fratzl, P.; Paris, O., On the Stability of Amorphous Minerals in Lobster Cuticle. *Advanced Materials* **2009**, 21 (40), 4011-4015.
14. Becker, A.; Ziegler, A.; Epple, M., The mineral phase in the cuticles of two species of Crustacea consists of magnesium calcite, amorphous calcium carbonate, and amorphous calcium phosphate. *Dalton Transactions* **2005**, (10), 1814-1820.
15. Shechter, A.; Berman, A.; Singer, A.; Freiman, A.; Grinstein, M.; Erez, J.; Aflalo, E. D.; Sagi, A., Reciprocal Changes in Calcification of the Gastrolith and Cuticle During the Molt Cycle of the Red Claw Crayfish *Cherax quadricarinatus*. *Biol. Bull. (Woods Hole)* **2008** 214, 122-134.
16. Plummer, L. N.; Busenberg, E., The solubilities of calcite, aragonite and vaterite in CO₂-H₂O solutions between 0 and 90°C, and an evaluation of the aqueous model for the system CaCO₃-CO₂-H₂O. *Geochimica et Cosmochimica Acta* **1982**, 46 (6), 1011-1040.
17. de Leeuw, N. H.; Parker, S. C., Surface structure and morphology of calcium carbonate polymorphs calcite, aragonite, and vaterite: An atomistic approach. *Journal of Physical Chemistry B* **1998**, 102 (16), 2914-2922.
18. Lippmann, F., *Sedimentary Carbonate Minerals*. Springer Verlag: Berlin, 1973.
19. Stanley, S. M., Effects of Global Seawater Chemistry on Biomineralization: Past, Present, and Future. *chemical reviews* **2008**, 108 (11), 4483-4498.

20. Baird, T.; Solomon, S. E., Calcite and aragonite in the egg shell of *Chelonia mydas* L. *Journal of Experimental Marine Biology and Ecology* **1979**, 36 (3), 295-303.
21. Checa, A. G.; Rodríguez-Navarro, A. B., Self-organisation of nacre in the shells of Pterioida (Bivalvia: Mollusca). *Biomaterials* **2005**, 26 (9), 1071-1079.
22. Heinemann, F.; Launspach, M.; Gries, K.; Fritz, M., Gastropod nacre: Structure, properties and growth — Biological, chemical and physical basics. *Biophysical Chemistry* **2011**, 153 (2–3), 126-153.
23. García-Gutierrez, D. I.; Jose-Yacamán, M.; Reyes-Gasga, J.; Velázquez-Castillo, R., Nanoscale characterization of nautilus shell structure: An example of natural self-assembly. *Journal of Materials Research* **2006**, 21 (6), 1484-1489.
24. Falini, G.; Albeck, S.; Weiner, S.; Addadi, L., Control of aragonite or calcite polymorphism by mollusk shell macromolecules. *Science* **1996**, 271 (5245), 67-69.
25. Lin, A.; Meyers, M. A., Growth and structure in abalone shell. *Materials Science and Engineering a-Structural Materials Properties Microstructure and Processing* **2005**, 390 (1-2), 27-41.
26. Sun, J.; Bhushan, B., Hierarchical structure and mechanical properties of nacre: a review. *RSC Advances* **2012**, 2 (20), 7617-7632.
27. Belcher, A. M.; Wu, X. H.; Christensen, R. J.; Hansma, P. K.; Stucky, G. D.; Morse, D. E., Control of crystal phase switching and orientation by soluble mollusc-shell proteins. *Nature* **1996**, 381, 56-58.
28. Falini, G.; Albeck, S.; Weiner, S.; Addadi, L., Control of aragonite or calcite polymorphism by mollusk shell macromolecules. *Science* **1996**, 271(5) (5245), 67-69.
29. Addadi, L.; Berman, A.; Oldak, J. M.; Weiner, S., Structural and Stereochemical Relations between Acidic Macromolecules of Organic Matrices and Crystals. *Connective Tissue Research* **1989**, 21 (1-4), 457-465.
30. Aizenberg, J.; Hanson, J.; Koetzle, T. F.; Leiserowitz, L.; Weiner, S.; Addadi, L., Biologically Induced Reduction in Symmetry - a Study of Crystal Texture of Calcitic Sponge Spicules. *Chemistry-a European Journal* **1995**, 1 (7), 414-422.
31. Albeck, S.; Aizenberg, J.; Addadi, L.; Weiner, S., Interactions of Various Skeletal Intracrystalline Components with Calcite Crystals. *Journal of the American Chemical Society* **1993**, 115 (25), 11691-11697.
32. Berman, A.; Addadi, L.; Kvick, A.; Leiserowitz, L.; Nelson, M.; Weiner, S., Intercalation of Sea-Urchin Proteins in Calcite - Study of a Crystalline Composite-Material. *Science* **1990**, 250 (4981), 664-667.
33. Heywood, B. R.; Mann, S., Template-Directed Nucleation and Growth of Inorganic Materials. *Advanced Materials* **1994**, 6 (1), 9-20.
34. Mann, S.; Archibald, D. D.; Didymus, J. M.; Douglas, T.; Heywood, B. R.; Meldrum, F. C.; Reeves, N. J., Crystallization At Inorganic-Organic Interfaces - Biominerals and Biomimetic Synthesis. *Science* **1993**, 261 (5126), 1286-1292.
35. Greenfield, E. M.; Crenshaw, M. A., Mineral Induction by the Soluble Matrix from Molluscan Shells. In *Origin, Evolution, and Modern Aspects of Biomineralization in Plants and Animals*, Crick, R. E., Ed. Springer US: Boston, MA, 1989; pp 303-308.
36. Gotliv, B. A.; Addadi, L.; Weiner, S., Mollusk shell acidic proteins: In search of individual functions. *Chembiochem* **2003**, 4 (6), 522-529.
37. Kong, J.; Liu, C.; Yang, D.; Yan, Y.; Chen, Y.; Liu, Y.; Zheng, G.; Xie, L.; Zhang, R., A novel basic matrix protein of *Pinctada fucata*, PNU9, functions as inhibitor during crystallization of aragonite. *CrystEngComm* **2019**, 21 (8), 1250-1261.
38. Takeuchi, T.; Sarashina, I.; Iijima, M.; Endo, K., In vitro regulation of CaCO₃ crystal polymorphism by the highly acidic molluscan shell protein Aspein. *Febs Letters* **2008**, 582 (5), 591-596.
39. Tsukamoto, D.; Sarashina, I.; Endo, K., Structure and expression of an unusually acidic matrix protein of pearl oyster shells. *Biochem Biophys Res Comm* **2004**, 320.
40. Kim, I. W.; Morse, D. E.; Evans, J. S., Molecular characterization of the 30-AA N-terminal mineral interaction domain of the biomineralization protein AP7. *Langmuir* **2004**, 20.
41. Collino, S.; Evans, J. S., Structural Features That Distinguish Kinetically Distinct Biomineralization Polypeptides. *Biomacromolecules* **2007**, 8 (5), 1686-1694.
42. Bahn, S. Y.; Jo, B. H.; Hwang, B. H.; Choi, Y. S.; Cha, H. J., Role of Pif97 in Nacre Biomineralization: In Vitro Characterization of Recombinant Pif97 as a Framework Protein for the Association of Organic-Inorganic Layers in Nacre. *Crystal Growth & Design* **2015**, 15 (8), 3666-3673.
43. Bahn, S. Y.; Jo, B. H.; Choi, Y. S.; Cha, H. J., Control of nacre biomineralization by Pif80 in pearl oyster. *Science Advances* **2017**, 3 (8).
44. Suzuki, M.; Saruwatari, K.; Kogure, T.; Yamamoto, Y.; Nishimura, T.; Kato, T.; Nagasawa, H., An Acidic Matrix Protein, Pif, is a Key Macromolecule for Nacre Formation. *Science* **2009**, 325 (5946), 1388-1390.
45. Metzler, R. A.; Evans, J. S.; Killian, C. E.; Zhou, D.; Churchill, T. H.; Appathurai, N. P.; Coppersmith, S. N.; Gilbert, P. U. P. A., Nacre Protein Fragment Templates Lamellar Aragonite Growth. *Journal of the American Chemical Society* **2010**, 132 (18), 6329-6334.
46. Yang, D.; Yan, Y.; Yang, X.; Liu, J.; Zheng, G.; Xie, L.; Zhang, R., A basic protein, N25, from a mollusk modifies calcium carbonate morphology and shell biomineralization. *Journal of Biological Chemistry* **2019**, 294 (21), 8371-8383.
47. Du, Y. P.; Chang, H. H.; Yang, S. Y.; Huang, S. J.; Tsai, Y. J.; Huang, J. J. T.; Chan, J. C. C., Study of Binding Interaction between Pif80 Protein Fragment and Aragonite. *Scientific Reports* **2016**, 6.

48. Futagawa, K.; Morioka, T.; Furihata, K.; Watanabe, H.; Ito, Y.; Ikeya, T.; Hokura, A.; Nagata, K.; Suzuki, M., Structural and Functional Analyses of the Acidic and Basic Amino Acid Repeat Sequence (DDRK) in Pif 80 from *Pinctada fucata* on the Aragonite Crystal Surface Using NMR. *Crystal Growth & Design* **2023**, 23 (7), 5264-5278.
49. Suzuki, M.; Iwashima, A.; Tsutsui, N.; Ohira, T.; Kogure, T.; Nagasawa, H., Identification and Characterisation of a Calcium Carbonate-Binding Protein, Blue Mussel Shell Protein (BMSP), from the Nacreous Layer. *ChemBioChem* **2011**, 12 (16), 2478-2487.
50. Day, D.; Lando, J. B., Morphology of Crystalline Diacetylene Monolayers Polymerized at the Gas-Water Interface. *Macromolecules* **1980**, 13, 1478-1483.
51. Lieser, G.; Tieke, B.; Wegner, G., Structure, Phase-Transitions and Polymerizability of Multilayers of Some Diacetylene Monocarboxylic Acids. *Thin Solid Films* **1980**, 68 (1), 77-90.
52. Wenzel, M.; Atkinson, G. H., Chromatic properties of polydiacetylene films. *J. Am. Chem. Soc.* **1989**, 111, 6123-6127.
53. Berman, A.; Ahn, D. J.; Lio, A.; Salmeron, M.; Reichert, A.; Charych, D., Total Alignment of Calcite At Acidic Polydiacetylene Films - Cooperativity At the Organic-Inorganic Interface. *Science* **1995**, 269 (5223), 515-518.
54. Sato, K.; Kumagai, Y.; Kogure, T.; Watari, K.; Tanaka, J., Polymorph and orientation controls of calcium carbonate crystals achieved by organic matrices. *Journal of the Ceramic Society of Japan* **2006**, 114 (1333), 754-759.
55. Lifshitz, Y.; Golan, Y.; Konovalov, O.; Berman, A., Structural Transitions in Polydiacetylene Langmuir Films. *Langmuir* **2009**, 25 (8), 4469-4477.
56. Gorna, K.; Hund, M.; Vucak, M.; Gršhn, F.; Wegner, G., Amorphous calcium carbonate in form of spherical nanosized particles and its application as fillers for polymers. *Materials Science and Engineering: A* **2008**, 477 (1-2), 217-225.
57. Nahi, O.; Kulak, A. N.; Zhang, S.; He, X.; Aslam, Z.; Ilett, M. A.; Ford, I. J.; Darkins, R.; Meldrum, F. C., Polyamines Promote Aragonite Nucleation and Generate Biomimetic Structures. *Advanced Science* **2023**, 10 (1), 2203759.
58. Wray, J. L.; Daniels, F., Precipitation of Calcite and Aragonite. *Journal of the American Chemical Society* **1957**, 79 (9), 2031-2034.
59. Cardew, P. T.; Davey, R. J., The Ostwald Ratio, Kinetic Phase Diagrams, and Polymorph Maps. *Crystal Growth & Design* **2019**, 19 (10), 5798-5810.